Spontaneous rupture processes on a bending fault

Y. Kase[1,2] and S. M. Day[1]

Received 27 January 2006; accepted 12 April 2006; published 18 May 2006.

[1] We simulated spontaneous rupture processes on a vertical, bending strike slip fault in a three-dimensional half space, using a finite-difference method. Rupture area and overall slip distribution on the fault vary with the initial stress field, which depends on strike change at the bend. Rupture velocity and detailed slip distribution around the bend, on the other hand, are affected by time-dependent normal stress change caused by rupture. This dynamic stress change plays an important role in the rupture process ahead of the bend, as well as in the resulting ground motion. The numerical simulation method demonstrated here in a simplified geometry is equally applicable to modeling strong ground motion from geometrically complex ruptures in realistic earth models. **Citation:** Kase, Y., and S. M. Day (2006), Spontaneous rupture processes on a bending fault, *Geophys. Res. Lett.*, *33*, L10302, doi:10.1029/2006GL025870.

1. Introduction

[2] Earthquake faults sometimes have bends, and the bends act as geometrical barriers to earthquake rupture [e.g., *King and Nábělek*, 1985]. In some recent studies, dynamic ruptures on a nonplanar fault were simulated numerically [e.g., *Bouchon and Streiff*, 1997]. *Aochi et al.* [2002] and *Kame et al.* [2003] showed that shear stress changes produced by the rupture front dominate during dynamic rupture propagation and that the rupture process depends strongly on the orientation of the fault system. In numerical studies of rupture jumps across jogs between fault segments [*Harris and Day*, 1999; *Kase and Kuge*, 2001], on the other hand, the jumps occur preferentially near the free surface. In part, this is because dynamic changes in normal stress may be large compared with initial stresses near the free surface. Therefore, the effect of dynamic normal stress change at a fault bend should be investigated in a model that includes a free surface. *Harris et al.* [2002] modeled the entire rupture including a bend with a finite-difference method and a transformation of coordinate system for the fault ahead the bend, but they did not deal with interaction between the different striking segments.

[3] The purpose of this study is to assess how dynamic normal stress perturbations induced by a fault bend affect the earthquake rupture process and resulting ground motion. To simulate spontaneous rupture processes on a bending fault in a three-dimensional half space, we use a finite-difference method. The fault follows a coordinate surface deformed to follow the fault strike, and we reformulate the equations of motion for the deformed system using a coordinate mapping.

2. Simulation Method

[4] We put a vertical fault in a 3-D, semi-infinite, homogeneous, isotropic, and linear elastic medium (Figure 1). The fault length and width are 30 km and 15 km, respectively. An initial crack is located at 7.5 km depth and 10 km along-strike distance from the end of the fault. The fault bends in the direction of θ at 10 km along-strike distance from the hypocenter.

[5] To calculate spontaneous rupture processes, we solve the elastic wave equations with boundary conditions for a fault plane and a free surface. On the fault surface, we introduce Coulomb friction, with a slip-weakening law for the friction coefficient [*Andrews*, 1976; *Day*, 1982]. Across the unruptured region on the fault, all components of traction and velocity are continuous. Slip starts at points where shear stress exceeds the static frictional stress that is equal to the static coefficient of friction times normal stress. On the ruptured region of the fault, all tractions, as well as the velocity components normal to the fault, are continuous across the fault plane, and total slip obeys the slip-weakening friction law, with the residual frictional strength given by the product of the compressive normal stress and a dynamic coefficient of friction.

[6] In our 3-D finite-difference scheme, we model the fault-strike change by mapping the parallelogram region along which the fault is located, onto a rectangular region. A similar method was applied to quasidynamic calculations of rupture processes with constant rupture velocity by *Inoue* [1996]. For spontaneous rupture simulations we find it advantageous to keep the grid interval on the fault uniform. Orthogonal coordinates (x, y, z) expressed in terms of an oblique coordinate system (ξ, η, ζ) are

$$x(\xi,\eta,\zeta) = \cos\theta\cdot\xi$$
$$y(\xi,\eta,\zeta) = \sin\theta\cdot\xi + \eta$$
$$z(\xi,\eta,\zeta) = \zeta.$$

Therefore, the spatial partial differential operators are transformed by

$$\frac{\partial}{\partial x} = \frac{1}{\cos\theta}\frac{\partial}{\partial\xi} - \tan\theta\frac{\partial}{\partial\eta}$$
$$\frac{\partial}{\partial y} = \frac{\partial}{\partial\eta}$$
$$\frac{\partial}{\partial z} = \frac{\partial}{\partial\zeta}.$$

By means of these operators, all equations of motion are replaced with corresponding equations in the oblique

[1]Department of Geological Sciences, San Diego State University, San Diego, California, USA.
[2]Now at Geological Survey of Japan, National Institute of Advanced Industrial Science and Technology, Ibaraki, Japan.

0094-8276/06/2006GL025870$05.00

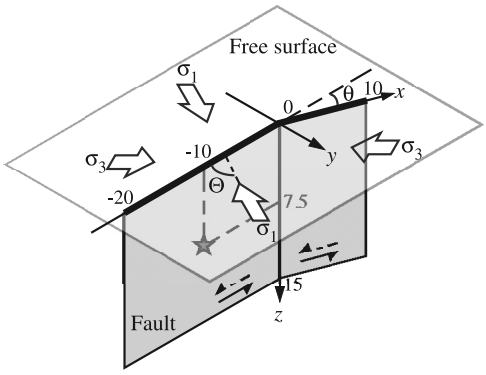

Figure 1. Numerical model used in this study. A star indicates the hypocenter.

coordinates. For example, the u_x component of the elastic wave equations is

$$\rho\frac{\partial^2 u_x}{\partial t^2} = (\lambda+2\mu)\frac{1}{\cos^2\theta}\frac{\partial^2 u_x}{\partial \xi^2} + \{(\lambda+2\mu)\tan^2\theta+\mu\}\frac{\partial^2 u_x}{\partial \eta^2} + \mu\frac{\partial^2 u_x}{\partial \zeta^2} + (\lambda+\mu)\frac{1}{\cos\theta}\frac{\partial^2 u_y}{\partial \xi\partial\eta} + (\lambda+\mu)\frac{1}{\cos\theta}\frac{\partial^2 u_z}{\partial\zeta\partial\xi} - (\lambda+2\mu)\frac{2\sin\theta}{\cos^2\theta}\frac{\partial^2 u_x}{\partial\xi\partial\eta} - (\lambda+\mu)\tan\theta\frac{\partial^2 u_y}{\partial\eta^2} - (\lambda+\mu)\tan\theta\frac{\partial^2 u_z}{\partial\eta\partial\zeta},$$

and the strike component of shear traction on a fault is

$$T_x = -2\mu\sin\theta\frac{\partial u_x}{\partial\xi} + \mu\frac{\partial u_x}{\partial\eta} + \mu\frac{\cos 2\theta}{\cos\theta}\frac{\partial u_y}{\partial\xi} + \mu\tan\theta\frac{\partial u_y}{\partial\eta},$$

where ρ is density, and λ and μ are Lame's elastic constants of medium. We solve these equations, using a finite-difference method with a conventional (unstaggered) grid.

[7] Stress conditions and coefficients of friction are assumed such that the maximum static stress drop (initial shear stress minus the product of initial normal stress and dynamic coefficient of friction) occurs on the part of the fault with the hypocenter (Table 1). The medium is subjected to principal compressional stresses (σ_1 and σ_3) proportional to depth (but independent of the horizontal coordinates). The initial stresses ahead of the bend therefore depend upon the bending angle, θ (Figure 2), and the stress drop is maximum in case $\theta = 0°$. The strength excess, defined as the difference between static frictional stress and initial shear stress, becomes larger when the fault strike change promotes compressional normal stress across the fault ($\theta > 0°$; "restraining bend"). On the other hand, strength excess initially decreases, reaches a minimum at $\theta = -6°$, and then increases, when the fault strike change promotes extensional normal stress ($\theta < 0°$; "releasing bend"). Therefore, we would expect releasing bends of small angle to be relatively favorable to rupture.

Table 1. Parameters Used in This Study[a]

	Variable	Unit	Value
Maximum principal stress	σ_1	MPa	11.278 z
Minimum principal stress	σ_3	MPa	4.622 z
Static coefficient of friction	μ_s		0.634
Dynamic coefficient of friction	μ_d		0.347
Angle between fault and σ_1	Θ	deg.	28.813
Critical displacement	D_c	m	0.25
P wave velocity		km/s	6.00
S wave velocity		km/s	3.46
Density	ρ	g/cm^3	2.67
Grid interval of space		km	0.25
Grid interval of time		s	0.025

[a] z is depth in km.

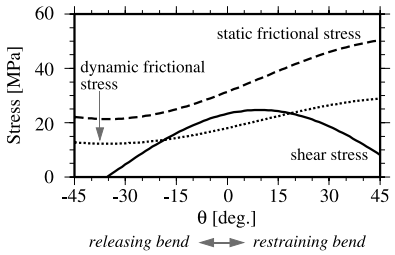

Figure 2. Dependence upon the bending angle, θ, of initial shear stress (solid line), initial static frictional stress (dashed line), and initial dynamic frictional stress (dotted line). The figure shows the stresses at 7.5 km depth.

3. Results

[8] Rupture velocity changes ahead of a bend, as well as the large-scale slip distribution over the fault, depend principally upon the initial strength excess and stress drop heterogeneities (Figure 2), which in turn are related to static stress variations induced by fault geometry. Disturbances of rupture velocity, as well as small-scale slip distribution near a bend, on the other hand, are caused principally by dynamic normal stress changes during rupture propagation. We show each individual feature, comparing rupture processes with those of a straight fault model (Figure 3a).

3.1. Effect of Static Stress Variation

[9] When a fault strike change promotes compressional normal stress across the fault (restraining bend), rupture velocity ahead of a bend decelerates (Figures 3b and 3c). When a fault strike slightly changes to promote extensional normal stress across the fault (releasing bend), rupture velocity accelerates at the bend, but then decelerates (Figure 3d). For a high bending angle case, rupture terminates ahead of the bend because of the large strength excess and negative stress drop beyond the bend (Figures 3c and 3e).

[10] The resulting slip distributions are consistent with the initial stress distributions. The amount of slip is maximum in the straight fault model (Figure 3a), since we assume initial stress conditions such that stress drop is maximum in case of $\theta = 0°$. In high bending-angle cases, slip is very small (Figures 3c and 3e) because the initial conditions imply negative stress drop (Figure 2). The relationship between bending angle and rupture process is consistent with rupture propagation and termination of real earthquakes: for example, in the 1999 Izmit earthquake, the surface slip decreased ahead of a 10°-releasing bend and the rupture terminated at a 20°-restraining bend [e.g., *Barka et al.*, 2002].

[11] We also simulated rupture propagation under other stress conditions. In all simulations, rupture velocity change

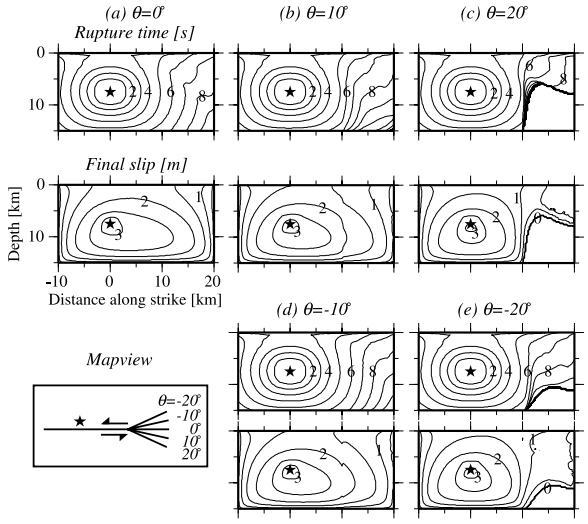

Figure 3. The figure tops show rupture time and the figure bottoms show slip distributions on (a) a straight fault, (b) a fault with a 10° restraining bend, (c) a fault with a 20° restraining bend, (d) a fault with a 10° releasing bend, and (e) a fault with a 20° releasing bend, respectively. Stars indicate hypocenter locations.

ahead of a bend and large-scale slip distribution on the fault can be understood qualitatively in a similar manner, in terms of initial strength excess and stress drop heterogeneities (Figure 2). This is consistent with *Aochi et al.* [2002].

3.2. Effect of Dynamic Normal Stress Change

[12] Before rupture, normal stress change ahead of the bend is small, and it does not play a dominant role in controlling subsequent rupture propagation across the bend. After rupture, on the other hand, large normal stress changes occur, and these cause variations of stress drop, with significant effects on the details of the slip distribution near the bend.

[13] Ahead of a restraining bend, normal stress (positive in compression) dynamically increases due to slip behind the bend (dotted grey line in Figure 4a). The increase in normal stress causes an increase in dynamic frictional stress (thick grey line in Figure 4a), which in turn causes a decrease in stress drop. Slip, therefore, is suppressed ahead of the bend (thin grey line in Figure 4a), as can be seen in Figures 3b and 3c. Behind the restraining bend, on the other hand, normal stress dynamically decreases due to slip ahead of the bend (a dotted black line in Figure 4a). The decrease in normal stress causes a decrease in dynamic frictional stress (thick black line in Figure 4a), which in turn causes an increase in stress drop. Slip behind the bend, therefore, is promoted (thin black line in Figure 4a).

[14] In a releasing bend, dynamic stress changes and their effects on the slip distribution are opposite to those in a restraining bend. Normal and dynamic frictional stresses decrease ahead of the bend (dotted and thick grey lines in Figure 4b), while they increase behind the bend (dotted and thick black lines in Figure 4b). Thus, slip ahead of a bend is promoted, while slip behind a bend is suppressed (thin grey and black lines in Figure 4b).

[15] The normal stress changes around a releasing bend are consistent with the results for a boundary integral equation model with abrupt kinks investigated by *Tada and Yamashita* [1996]. They pointed out the apparent paradox that normal stress changes on a smooth curved fault have opposite sign from those on a fault with an abrupt kink. To the extent that real faults have many small, abrupt kinks, we would expect normal stress changes during rupture (and the resulting effects on slip distribution) to be comparable to those described in this section. Finite element studies by *Oglesby et al.* [2003] and *Duan and Oglesby* [2005] showed similar time-dependent effects of normal stress change near bends.

4. Can We Use No-Bending Fault Model Instead of Bending Fault?

[16] In the previous section, we showed that static stress variations affect the rupture process ahead of a bend and dynamic normal stress changes affect the rupture process in the immediate vicinity of the bend. Static stress variations can be included in initial stress conditions, without the computational complications that accompany the bent fault geometry. Therefore, we briefly assess the viability of approximating the dynamics of a bending fault by replacing it with a straight fault subjected to the same initial stresses: Can initial stress heterogeneity be substituted for a bending fault model?

[17] We compare results of two models. The first has a fault with a 10°-clockwise bend at 10 km along-strike distance from the hypocenter in a homogeneous stress field (bending fault model). The second has a straight fault in a heterogeneous stress field such that the horizontal principal stress axes rotate 10°-counterclockwise, beginning 10 km along-strike distance from the hypocenter (straight fault model). In the both models, initial shear and normal stress distributions on the faults are the same.

[18] A rupture propagates more slowly ahead of the bend in the bending fault model than it does ahead of the stress-rotation point in the straight fault model (Figure 5a). The rupture decelerates ahead of the bend, due to dynamic normal stress increases, as discussed previously. The decrease of rupture velocity is clear in the shallow portion.

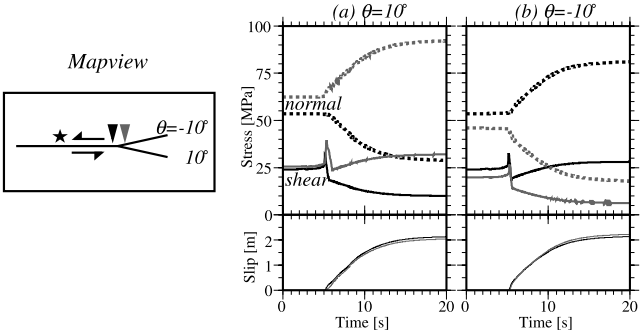

Figure 4. Time histories of slip (thin lines), shear stress (thick lines) and normal stress (dotted lines) at 9.75 km (just behind bends; black lines) and 10.25 km (just ahead of bends; grey lines) along strike distance from the hypocenter. (a) Fault with a 10° restraining bend. (b) Fault with a 10° releasing bend.

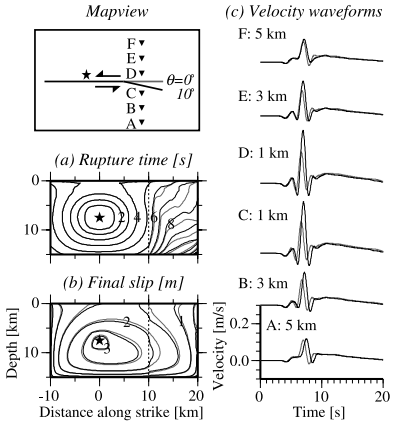

Figure 5. Comparison of (a) rupture time, (b) slip distribution, and (c) fault-normal component of 1 Hz low-pass-filtered velocity waveforms in case of a 10°-bending fault under a horizontally homogeneous stress field (black lines) and in case of a straight fault under a horizontally heterogeneous stress field (grey lines). In the both cases, initial shear and normal stress distributions on the faults are the same. The Figure 5c stations are located at (A) 5 km, (B) 3 km, (C) 1 km on fault-bending side, (D) 1 km, (E) 3 km, (F) 5 km in the opposite side from a point at 5 km along strike distance from the bend.

Since stresses assumed in this study are proportional to depth, the dynamic stress disturbance due to rupture is dominant over the applied static stress in the shallow portion. Therefore, rupture deceleration is easily caused by normal stress increase, and the rupture propagation direction is deflected downward. Slip distribution is smoother in straight fault model than in bending fault model, because of the absence of dynamic normal stress change around the bend (Figure 5b).

[19] We also compare velocity waveforms in both models. Near the bend, the amplitude of the fault-normal component is larger in the bending fault model than in the straight fault model (Figure 5c), although the slip on the fault is smaller (Figure 5b). Thus, there is a non-negligible effect of fault geometry on the fault-normal velocity, at least in the immediate vicinity of the bend.

[20] The rupture process ahead of the stress-rotation point in the straight fault model is different in detail from that in bending fault model, suggesting the possibility that the character of rupture heterogeneity could be an aid to inferring underground fault geometry. Moreover, a straight fault model underestimates ground motion near a fault bend. Improved modeling of fault geometry in dynamic rupture simulations may therefore aid the physical interpretation of strong ground motion observations and lead to more realistic ground motion predictions, although, in practice, the effects of geometry may be difficult to separate from those of stress heterogeneity.

5. Conclusion

[21] We simulated spontaneous rupture processes on a vertical, bending fault, using a three-dimensional finite-difference method. Rupture area and large-scale slip distribution over the fault vary with strike change, since initial shear and normal stresses on the fault depend upon the angle of the fault to the principal stresses. Rupture velocity and detailed slip distribution around a bend, on the other hand, are affected by normal stress change caused by rupture, which leads to predicted rupture process and ground motion which differ from those of a straight fault under the same heterogeneous static stress condition. The methods demonstrated here for simple rupture models can also be applied to incorporate irregular fault geometry into more realistic dynamic simulations of strong ground motion generation from large earthquakes.

[22] **Acknowledgments.** We thank R.A. Harris for her thoughtful reviews. One of us (Y.K.) was supported by Research Fellowships of the Japan Society for the Promotion of Science for Young Scientists. The work was also supported by the National Science Foundation, under grants ATM-0325033, and by the Southern California Earthquake Center (SCEC). SCEC is funded by NSF Cooperative Agreement EAR-0106924 and USGS Cooperative Agreement 02HQAG0008. The SCEC contribution number for this paper is 950. We used the GMT (Generic Mapping Tool version 3.4) [*Wessel and Smith*, 1998] for drawing some figures.

References

Andrews, D. J. (1976), Rupture velocity of plane strain shear cracks, *J. Geophys. Res.*, *81*, 5679–5687.

Aochi, H., R. Madariaga, and E. Fukuyama (2002), Effect of normal stress during rupture propagation along nonplanar faults, *J. Geophys. Res.*, *107*(B2), 2038, doi:10.1029/2001JB000500.

Barka, A., et al. (2002), The surface rupture and slip distribution of the 17 August 1999 Izmit earthquake (M7.4), North Anatolian fault, *Bull. Seismol. Soc. Am.*, *92*, 43–60.

Bouchon, M., and D. Streiff (1997), Propagation of a shear crack on a nonplanar fault: A method of calculation, *Bull. Seismol. Soc. Am.*, *87*, 61–66.

Day, S. M. (1982), Three-dimensional simulation of spontaneous rupture: The effect of nonuniform prestress, *Bull. Seismol. Soc. Am.*, *72*, 1881–1902.

Duan, B., and D. D. Oglesby (2005), Multicycle dynamics of nonplanar strike-slip faults, *J. Geophys. Res.*, *110*, B03304, doi:10.1029/2004JB003298.

Harris, R. A., and S. M. Day (1999), Dynamic 3D simulations of earthquakes on en echelon faults, *Geophys. Res. Lett.*, *26*, 2089–2092.

Harris, R. A., J. F. Dolan, R. Hartleb, and S. M. Day (2002), The 1999 Izmit, Turkey, earthquake: A 3D dynamic stress transfer model of intraearthquake triggering, *Bull. Seismol. Soc. Am.*, *92*, 245–255.

Inoue, T. (1996), Near-fault ground motion prediction based on dynamic rupture simulations, Master thesis, Univ. of Tokyo, Tokyo.

Kame, N., J. R. Rice, and R. Dmowska (2003), Effect of prestress state and rupture velocity on dynamic fault branching, *J. Geophys. Res.*, *108*(B5), 2265, doi:10.1029/2002JB002189.

Kase, Y., and K. Kuge (2001), Rupture propagation beyond fault discontinuities: Significance of fault strike and location, *Geophys. J. Int.*, *147*, 330–342.

King, G., and J. Nábělek (1985), Role of fault bends in the initiation and termination of earthquake rupture, *Science*, *228*, 984–987.

Oglesby, D. D., S. M. Day, Y.-G. Li, and J. E. Vidale (2003), The 1999 Hector Mine earthquake: The dynamics of a branched fault system, *Bull. Seismol. Soc. Am.*, *93*, 2459–2476.

Tada, T., and T. Yamashita (1996), The paradox of smooth and abrupt bends in two-dimensional in-plane shear-crack mechanics, *Geophys. J. Int.*, *127*, 795–800.

Wessel, P., and W. H. F. Smith (1998), New, improved version of Generic Mapping Tools released, *Eos Trans. AGU*, *79*, 579.

S. M. Day, Department of Geological Sciences, San Diego State University, 5500 Campanile Drive, San Diego, CA 92182–1020, USA. (day@moho.sdsu.edu)

Y. Kase, Geological Survey of Japan, National Institute of Advanced Industrial Science and Technology, AIST Tsukuba Central 7, Ibaraki 305-8567, Japan. (kasep@ni.aist.go.jp)